INITIAL DEVELOPMENT OF THE HYBRID SEMIELLIPTICAL-DOLPHIN AIRFOIL

by

Zorana Z. DANČUO[a*], Ivan A. KOSTIĆ[b], Olivera P. KOSTIĆ[b], Aleksandar Č. BENGIN[b], and Goran S. VOROTOVIĆ[b]

[a] Innovation Center, Faculty of Mechanical Engineering, University of Belgrade, Belgrade, Serbia
[b] Aeronautical Department, Faculty of Mechanical Engineering, University of Belgrade, Belgrade, Serbia

Original scientific paper
https://doi.org/10.2298/TSCI210515234D

Iosif Taposu has formulated a mathematical model and generated a family of airfoils whose geometry resembles the dolphin shape. These airfoils are characterized by a sharp leading edge and experiments have proven that they can achieve better aerodynamic characteristics at very high angles of attack than certain classical airfoils, with the nose geometry inclined downwards. On the other hand, they have not been applied to any commercial general aviation aircraft. The authors of this paper have been motivated to compare the aerodynamic characteristics of widely used NACA 2415 airfoil with Taposu's Dolphin that would have the same principal geometric characteristics. A CFD calculation model has been established and applied on NACA 2415. The results were compared with NACA experiments and very good agreements have been achieved in the major domains of lift and polar curves. The same CFD model has been applied on the counterpart Dolphin 2415. Results have shown that the Dolphin has a slightly higher lift/drag ratio in the lift coefficient domain 0.1-0.35 than NACA. On the other hand, at higher and lower lift coefficients, its aerodynamic characteristics were drastically below those of the NACA section, due to the unfavorable influence of the Dolphin's sharp nose. A series of the Dolphin's leading edge modifications has been investigated, gradually improving its aerodynamics. Finally, version M4, consisting of about 70% of Dolphin's original rear domain and 30% of the new nose shape, managed to exceed the NACA's characteristics, thus paving the way to investigate the Dolphin hybrids that could be suitable for the general aviation industry.

Key words*: Dolphin airfoil, leading edge modification, hybrid design, computational aerodynamics, turbulence*

Introduction

The need to design novel airfoils with improved characteristics has always been an aspiration of aerodynamicists. Achieving the highest possible lift-to-drag ratio (L/D, or C_L/C_D ratio), improvement of the aerodynamic efficiency, avoiding flow separation at high inflow angles, stall delay*, etc.*, are of primary importance in creating modern concepts of airfoils. Consequently, men often find inspiration for discoveries and solutions in nature. Even more, engineering is interdependent with nature and its laws.

In the middle of the last century, the terms bionics and biomimetics were coined by Jack Steel, and Otto Schmitt. Bionics, *i.e*. Biomimetics refers to the practical use of biological

* Corresponding author, e-mail: zorana.dancuo@gmail.com

mechanisms and functions in science, engineering, electronics, design, *etc*. [1]. The authors of this paper were inspired by the fact that more and more researchers are trying to implement the body shapes of aquatic mammals, such as Dolphins, in the design of new airfoil concepts. Therefore, the research presented in this paper aims to contribute to the development of new bioinspired airfoils and to present a new hybrid semielliptical-Dolphin airfoil.

Dolphins are, however, not a new concept in aeronautical engineering. Sir George Cayley was the first to introduce the shape of a dolphin's body into aeronautics (around 1800). He envisioned this shape for the construction of a fuselage [2]. During the last few years, Chinese scientists, Huang *et al*. [3] have achieved remarkable results in terms of improving the aerodynamic characteristics based on the biomimetics of the head of a dolphin species – *Phocoenoides dalli*. Namely, Huang *et al.* [3] modified the symmetrical airfoil NACA 0018, by changing its leading edge. The NACA 0018 airfoil is used as the original airfoil, and tracing points of the *Phocoenoides dalli* head contour are added on the leading edge. The NACA 0018 is moved towards the mentioned contour until tangency was reached. In this way, a new bionic profile was obtained, whose modifications developed three more types of bionic Dolphin airfoils, moreover five subgroups.

An interesting new concept of airfoils, inspired by the shape of dolphins, was given by the Romanian scientist Iosif Taposu. Taposu proposed a completely new mathematical model for airfoils whose geometry irresistibly resembles the shape of a dolphin. The author suggests that these airfoils have higher performances compared to classical airfoils. The ideal Dolphin airfoil is defined with the tangency condition of one-half thickness distribution the skeleton line, in the leading and trailing edges. In his study about the experimental results of a Dolphin airfoil at low speeds, a comparison between groups of classical airfoils and the new Dolphin-concept was made at close Reynolds numbers. The Dolphin airfoil DA20G08 was compared to a group of classical airfoils named BLOC. Later on, DA20G08 was compared to a new set of classical airfoils – Joukovski's airfoil, NACA 0012, and Clark [4, 5].

Taposu's Dolphin concept was also analyzed by Berbente and Danaila [6]. The study is based on the enhancement of the Dolphin airfoil concept, by generating an airfoil while maintaining curvature continuity, and investigating how the airfoil's shape affects the aerodynamic characteristics.

Many researchers are nowadays occupied with airfoil optimization. Genetic algorithms, class-shape transformation or CST parametrization, and other methods are used, along with different turbulence models, in comparison with experimental data, to give the best results in the selection of the best airfoil shape [7]. Single- and multi-point aerodynamic optimizations are also used in unmanned air vehicles. The aim is to design aerodynamic shapes with lower drag than the initial shape [8]. In a very interesting study, through aerodynamic optimization, the whole front part of a guided missile was modified, while the rear part remained the same, very similar to the Dolphin airfoil in this paper [9]. As one can see, airfoil optimization is a crucial part of the contemporary high quality aerodynamic design, which is the primary goal of this paper as well.

Having all this in mind, the authors of this study decided to make a comparison between a Dolphin airfoil generated according to Taposu's mathematical algorithm, and a classical NACA airfoil, based on the match of the most relevant geometrical characteristics. For comparisons, the NACA 2415 airfoil has been adopted. According to the NACA four digit airfoil series, the numbers represent, respectively: its maximum camber of 2%, located at 40% of the chord, and the maximum thickness ratio of 15%, positioned by default at 30% of the chord. The Dolphin airfoil has been designed with the same principal geometric parameters.

A CFD model has been established and adopted, and it has initially been verified by comparisons with experimental data for NACA 2415 [10]. Using the same CFD model, the Dolphin airfoil has been analyzed. Several leading edge modifications of the Dolphin airfoil have been analized in order to improve its original aerodynamic characteristics, and one of them managed to exceed the aerodynamic characteristics of the original NACA 2415 showing that the Dolphin's airfoil hybrids could be suitable for the general aviation industry.

Generation of the original Dolphin airfoil geometry

In this section, the mathematical model for the Dolphin airfoil according to Taposu [4, 5] is briefly explained. The profile is determined with four main functions in Cartesian co-ordinates, in the *Oxz* plane: the skeleton-line distribution function along the *x*-axis, $s(x)$, eq. (1), the function of the half-thickness distribution along the *x*-axis, $g(x)$, eq. (3), the function of the suction and pressure surface, respectively, $z_e(x)$, $z_i(x)$, eq. (5) [5]:

$$\begin{gathered} s(x)=\phi_1 \text{ for } 0\le x\le \zeta_1,\ s(x)=\phi_2 \text{ for } \zeta_1 < x\le x_\zeta,\ s(x)=\phi_3 \text{ for } x_\zeta < x\le \zeta_2 \\ s(x)=\phi_4 \text{ for } \zeta_2 < x\le 1 \end{gathered} \tag{1}$$

where

$$\begin{gathered} \phi_1(x)=x\tan\alpha,\ \phi_2(x)=\xi-\frac{\left(x-x_\zeta\right)^2\tan\alpha}{2\left(x_\zeta-\zeta_1\right)},\ \phi_3(x)=\xi-\frac{\left(x-x_\zeta\right)^2\tan\beta}{2\left(\zeta_2-x_\zeta\right)} \\ \phi_4(x)=(1-x)\tan\beta \end{gathered} \tag{2}$$

$$\begin{gathered} g(x)=\varepsilon G_1 \text{ for } 0\le x\le x_1,\ g(x)=\varepsilon G_2 \text{ for } x_1 < x\le x_\varepsilon,\ g(x)=\varepsilon G_3 \text{ for } x_\varepsilon < x\le x_2 \\ g(x)=\varepsilon G_4 \text{ for } x_2 < x\le 1 \end{gathered} \tag{3}$$

where

$$\begin{gathered} G_1(x)=\frac{\varepsilon x^2}{\varepsilon_1 x_\varepsilon^2},\ G_2(x)=1-\frac{\varepsilon\left(x-x_\varepsilon\right)^2}{x_\varepsilon^2\left(\varepsilon-\varepsilon_1\right)},\ G_3(x)=1-\frac{\varepsilon\left(x-x_\varepsilon\right)^2}{\left(\varepsilon-\varepsilon_2\right)\left(x_\varepsilon-1\right)^2} \\ G_4(x)=\frac{\varepsilon\left(x-1\right)^2}{\varepsilon_2\left(x_\varepsilon-1\right)^2} \end{gathered} \tag{4}$$

and

$$z_e(x)=s(x)+g(x),\ z_i(x)=s(x)-g(x) \tag{5}$$

where coefficients are obtained

$$\begin{gathered} \beta=\tan^{-1}\left[\left(\frac{x_\zeta}{1-x_\zeta}\right)\tan\alpha\right],\ \zeta_1=\frac{2\zeta}{\tan\alpha}-x_\zeta,\ \zeta_2=2-x_\zeta-\frac{2\zeta}{\tan\beta} \\ x_1=\frac{\varepsilon_1 x_\varepsilon}{\varepsilon},\ x_2=1-\frac{\varepsilon_2\left(1-x_\varepsilon\right)}{\varepsilon},\ \varepsilon_1=\frac{2\varepsilon}{3},\ \varepsilon_2=\frac{\varepsilon}{3} \end{gathered} \tag{6}$$

and the aforementioned notations represent, respectively: x_ζ is the position of the maximum camber along the *x*-axis, α – the incidence angle, x_ε – the position of the maximum thickness along the *x*-axis, and ε – the half- thickness of the airfoil [5].

The skeleton line distribution function $s(x)$, eq. (1), and the function of the half-thickness distribution $g(x)$, eq. (3), are piecewise functions along the x-axis, *i.e.* chord of the Dolphin airfoil. The curve $g(x)$ can be divided into four parts, to get a better insight into the airfoil geometry: the first part – *the leading edge*, the second part – *previous ridge*, the third part – *rear ridge*, and the fourth part – the trailing edge [5].

Using this algorithm, the geometry *original Dolphin 2415* airfoil has been generated, with maximum camber ratio of 2%, located at 40% of the chord, and the maximum thickness ratio of 15%, positioned at 30% of the chord. With these basic geometric parameters, it is compatible with the NACA 2415, a widely used airfoil in the general aviation airplane category for many decades, fig. 1.

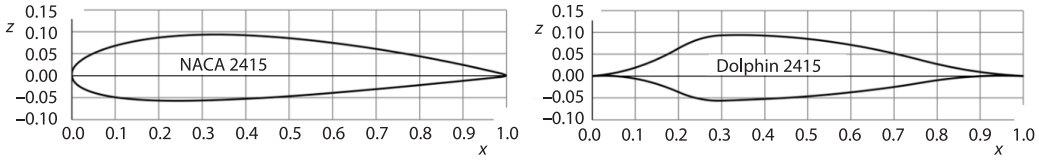

Figure 1. The NACA 2415 airfoil and the original Dolphin 2415 airfoil geometry

Aerodynamic comparison of the NACA 2415 and the original Dolphin 2415 airfoils

Computational algorithm

The computational analyses were performed in ANSYS FLUENT, using the RANS model, based on the Reynolds-averaged Navier–Stokes equations. The model represents time averaged equations of fluid motion. A two-equation SST k-ω (shear stress transport) turbulence model [11-14] has been selected, which can be expressed:

$$\frac{\partial(\rho k)}{\partial t}+\frac{\partial(\rho U_j k)}{\partial x_j}=P-\beta^*\rho\omega k+\frac{\partial}{\partial x_j}\left[(\mu+\sigma_k\mu_t)\frac{\partial k}{\partial x_j}\right] \tag{7}$$

$$\frac{\partial(\rho\omega)}{\partial t}+\frac{\partial(\rho u_j\omega)}{\partial x_j}=\frac{\gamma}{\nu_t}P-\beta\rho\omega^2+\frac{\partial}{\partial x_j}\left[(\mu+\sigma_\omega\mu_t)\frac{\partial\omega}{\partial x_j}\right]+2(1-F_1)\frac{\rho\sigma\omega_2}{\omega}\frac{\partial k}{\partial x_j}\frac{\partial\omega}{\partial x_j} \tag{8}$$

The SST model uses a blending function to apply the k-ω model near the surface, and k-ε model in free shear domains. As a result, the SST model has shown good experimental agreements for flows with adverse pressure gradients [8], which are commonly present in aerodynamic design. The 2-D density-based calculations were performed, using air as fluid with viscosity defined by the three coefficient Sutherland law. For viscous and convective terms in governing equations the second order discretization was implemented. The full multi-grid initialization of the solution [15] was employed, and solution steering for Courant number optimum settings. Such computational approach has been previously applied (with addition of compressibility terms and effects), in the calculations of very complex subsonic/supersonic flow patterns, where very good agreements with experiments were achieved [15-17]. The authors have decided to adopt it for here presented calculations as well, using the same initial and boundary conditions for all cases. The outlet was set to *pressure outlet*, inlet to *pressure-far-field*, with operating pressure p = 101325 Pa, temperature T = 288.15 K (standard sea level values) and the free-stream Mach number M = 0.2564, these values actually correspond the experimental Re = $6.0 \cdot 10^6$ and unit airfoil chord length, used for CFD verifications in the next section. The overall length and height of the control volume are equal to 25 airfoil chord lengths.

Experimental verification of the adopted CFD computational algorithm

The first step in these investigations was to verify the presented calculation model for applications on external flows around airfoils at lower subsonic Mach numbers. The CFD calculations of the lift and drag coefficients for the NACA 2415 airfoil were compared with the corresponding wind tunnel test data for this airfoil, obtained by NACA [7]. The *standard roughness* case was analyzed, where early transition of the laminar to turbulent boundary-layer is forced. It is less favorable than the natural transition case due to higher drag, but it is unfortunately a more common case in the operational use of general aviation aircraft. The unit chord airfoil and flow parameters corresponding to the experimental Re = 6.0 million were implemented in the CFD calculations. Structured C-grids with up to 300000 elements were tested, and a C-mesh with 115600 elements, fig. 2, proved to be optimal for those analyses, considering its complexity, obtained convergence rates and accuracy of the results.

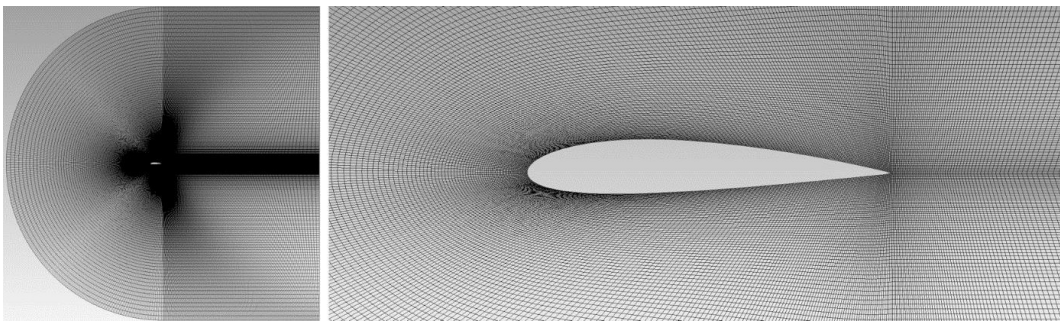

Figure 2. The C-mesh with 115600 elements and its distribution in the vicinity of the NACA 2415

Comparisons between the calculated and experimental curves, fig. 3, show very good agreements in major part of the analyzed α domain which is crucial for practical applications, except the fact that CFD calculations have partially overestimated the lift coefficient values in the vicinity of α_{cr}. Keeping in mind a very high time and resource efficiency of modern computers used in CFD analyses, compared to wind tunnels, and the fact that exactly the same computational and mesh generation algorithms will be implemented in all here presented CFD investigations, this computational model has been assessed as suitable tool for the initial development and analyses of Dolphin airfoil modifications.

Computational analysis of the original Dolphin 2415 airfoil

During CFD analyses, the original Dolphin 2415 airfoil has been subjected to the same inlet conditions as those implemented for NACA 2415 in previous chapter. Comparisons of the calculated lift and polar curves, and lift-to-drag ratios for the two airfoils are shown in fig. 4.

The quantitative aspect of the obtained results showed that the only advantage of Dolphin 2415 over NACA 2415 is slightly higher C_L/C_D ratio in the lift coefficient range $C_L \approx 0.1\text{-}0.35$, fig. 4(a), which corresponds to the cruising flight values. It means that in cruise, the original Dolphin could provide just a bit more economical flight (airfoil values directly influence the wing values). On the other hand, the original Dolphin's $C_{L,\max}$ is only some 60% of the calculated $C_{L,\max}$ of NACA 2415. It means that the same airplane with the original Dolphin would have a 30% higher stalling speed than with the NACA airfoil, which would be a disadvantage. The Dolphin's drag divergence starts very early, fig. 4(b). Because of that, the

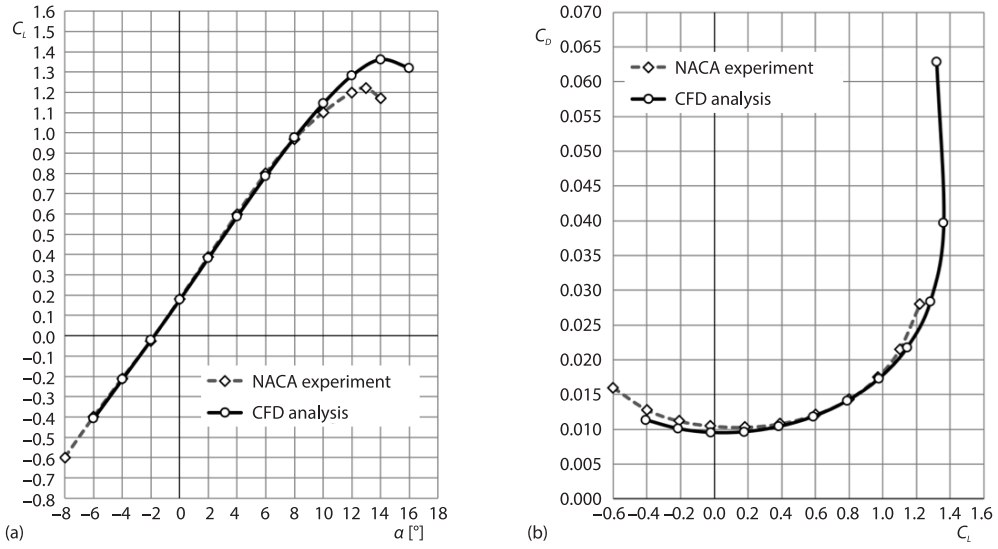

Figure 3. Experimental lift and polar curves for the NACA 2415 airfoil at Re = 6.0 · 10⁶ [7], and curves obtained by here presented CFD calculation model; (a) lift coefficient, standard roughness and (b) polar curves, standard roughness

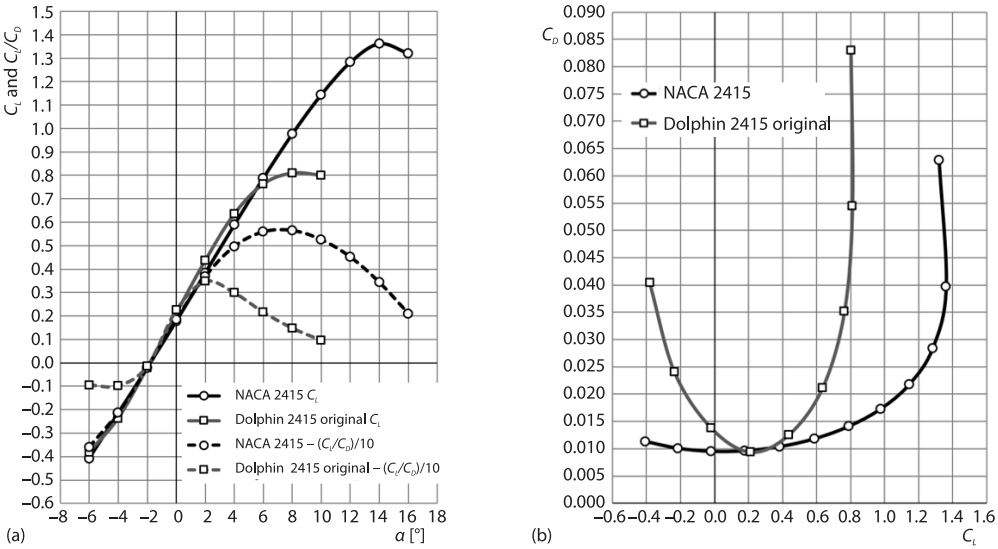

Figure 4. Lift curves, lift/drag ratios, and polar curves for NACA 2415 and original Dolphin 2415; (a) lift coefficient and lift/drag ratio and (b) polar curves, standard roughness

Dolphin's $(C_L/C_D)_{max}$ value is about 40% lower than this value for NACA. As a consequence, the maximum possible range of a piston engined airplane (flight at a smaller cruising speed, which corresponds to the lift coefficient for $(C_L/C_D)_{max}$ – see also tab. 1) with Dolphin airfoil would be 40% smaller than with NACA 2415, which would also be a substantial drawback. These might be the two important reasons why airfoils such as the here analyzed original Dolphin have not been applied on the commercial general aviation airplanes so far.

The most important aspect of the qualitative comparative analyses of the two airfoils is presented in fig. 5, in the terms of the flow field's velocity contours for several representative angles of attack, up to the critical angles of attack, which are remarkably different for the two airfoils.

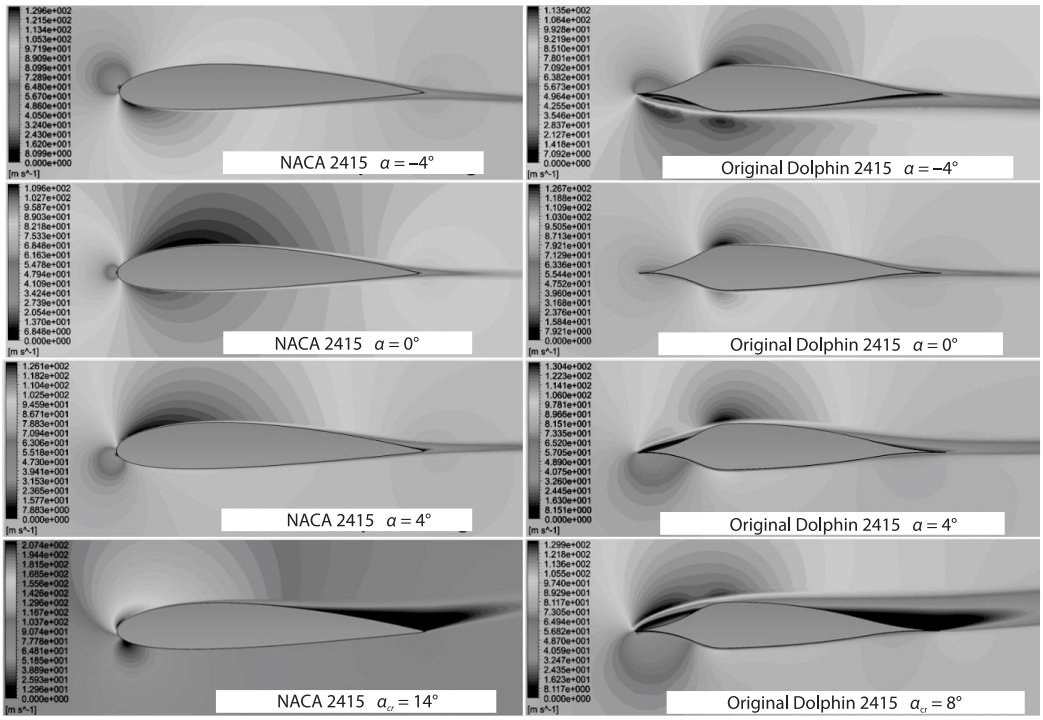

Figure 5. Velocity contours calculated for angles of attack $\alpha = -4°$, $\alpha = 0°$, $\alpha = 4°$ and the critical angles of attack $\alpha_{cr} = 14°$ for NACA, and $\alpha_{cr} = 8°$ for the original Dolphin airfoil

From the velocity contours it is obvious that NACA 2415 preserves very smooth flow patterns around the leading edge at all angles of attack, with the front stagnation point (*i.e.* the contact point between the small *sphere* and the airfoil contour in its nose domain) freely adopting its natural position on its rounded nose, depending on the angle of attack. Its stall angle is characterized only by the trailing edge separation wake, while flow about the nose remains attached to the airfoil contour.

On the other hand, except at $\alpha \approx 0°$, even at small angles of attack $\alpha = \pm 4°$ the strong leading edge separation from the dolphin's sharp nose is noticeable, which decreases the lift and increases the drag. At its $\alpha_{cr} = 8°$, beside the trailing edge separation wake, a very strong leading edge separation bubble is visible, contributing to an early separation and thus correspondingly small $C_{L,\max}$ value. These unfavorable effects are the consequence of the sharp leading edge, which forces the front stagnation point to remain fixed at this position. Then the air-flow naturally *rounds* the nose of the airfoil by generating the leading edge separation bubbles, which degrade aerodynamic characteristics of the original Dolphin airfoil. An obvious approach, with an aim to improve the original dolphin's lift and drag characteristics in a wider range of angles of attack, was to modify its nose domain.

Development and analysis of the new hybrid semielliptical-Dolphin airfoil

The first modification: denoted as Dolphin 2415 M1, was inspired by the dark air-flow separation zones below and above the dolphin's nose at the angles of attack $\alpha = -4°$ and $\alpha = +4°$, fig. 5. Instead of a sharp nose, the leading edge radius was assigned, as 1/3 of the standard NACA 4 digit airfoil series nose radius [7], and the obtained value was $(r/c)_0 = 0.00826425$. It was merged with the original airfoil by the tangents drawn from it to the points $x = 0.15$, $z = 0.0381250$, and $x = 0.15$, $z = -0.0181250$. The obtained geometry has preserved the obvious *dolphin-like* shape (fig. 6, with contour presented in the calculation mesh environment). With the same inlet inputs as in previous two chapters, the CFD calculations have shown that the M1 had about 10% larger $C_{L,\max}$ value, 30% larger $(C_L/C_D)_{\max}$ and the drag divergence zone shifted to the right, fig. 7, compared to the original Dolphin 2415. Improvements were obvious, but M1 was still far from becoming a counterpart for NACA 2415.

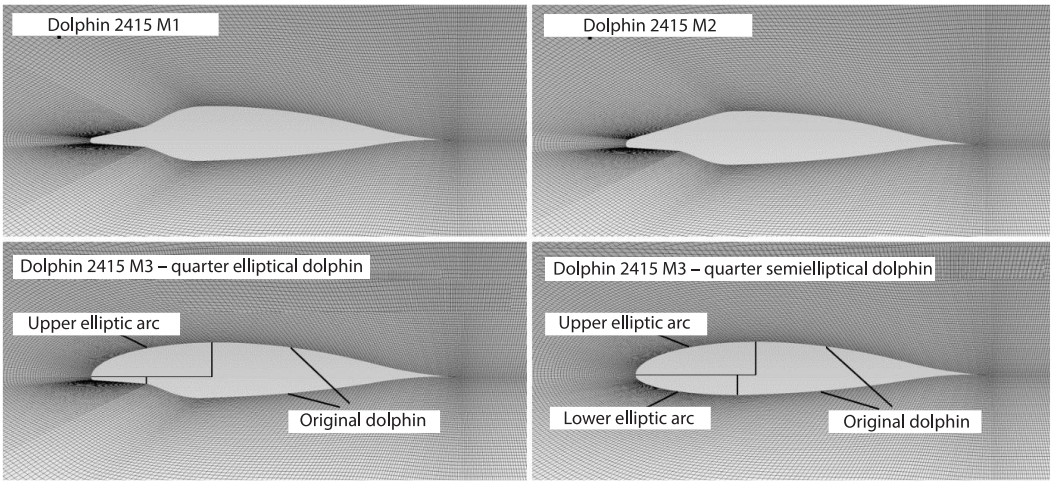

Figure 6. New versions have been analyzed on similar C-mesh type with 115600 elements as the mesh used for NACA 2415 airfoil, adjusted for the actual Dolphin's modification geometry

The second modification: the Dolphin 2415 M2 was inspired by the clearly defined, sharp white vortex emerging from the original Dolphin's leading edge at $\alpha = +4°$, fig. 5. It defines the outer layer of air-flow above the leading edge domain, through which the aerodynamic forces have performed the *natural optimization* of the airfoil geometry for the given angle of attack. It touches the top of the upper airfoil camber. In that sense, the upper surface leading edge radius on M2 was increased to 2/3 of the standard NACA 4 digit airfoil series radius, giving $(r/c)_0 = 0.0165285$. It was merged with the upper camber of the original airfoil by its tangent to the point $x = 0.25$, $z = 0.08500$, while the lower side modification was the same as on M1, fig. 6. This version has provided further aerodynamic improvements compared to the original dolphin values, giving this time 34% larger $C_{L,\max}$, 77% larger $(C_L/C_D)_{\max}$ and the drag divergence zone was noticeably shifted to the right, fig. 7. The M2 $(C_L/C_D)_{\max}$ was only 5% smaller than of the NACA 2415, but its $C_{L,\max}$ was still 20% lower than the $C_{L,\max}$ of the NACA airfoil.

The third modification: the Dolphin 2415 M3 was focused on the increase of the $C_{L,\max}$. Inspired by the flow pattern shown in fig. 5 for the original Dolphin at $\alpha_{cr} = 8°$, the additional upper camber curvature in the wider nose domain seemed to be required. The decision was made to apply an elliptic arc, starting from the leading edge up to the maximum point of the upper original Dolphin airfoil camber, defined by co-ordinates $x = 0.34$ and $z = 0.0940327$, where

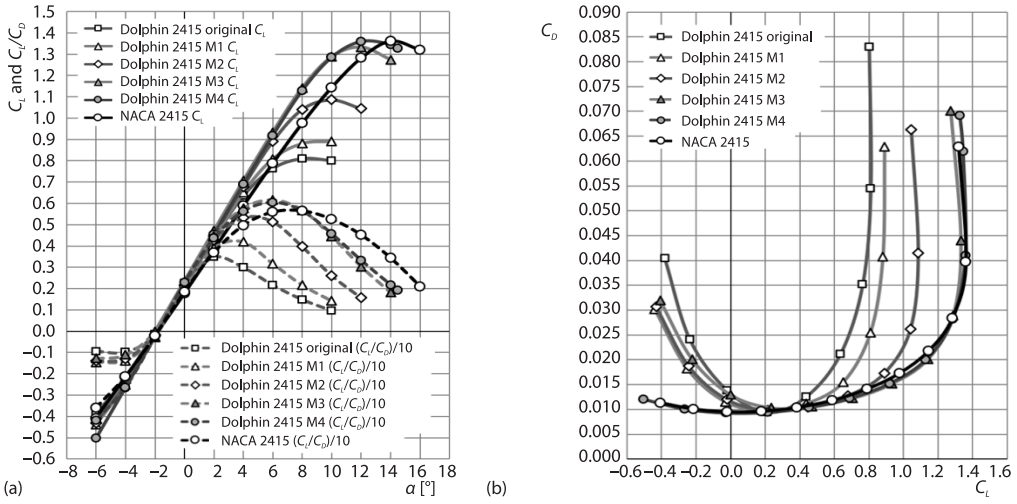

Figure 7. Comparisons of NACA 2415 airfoil and different Dolphin 2415 versions; (a) lift coefficient and lift/drag ratio and (b) polar curves, standard roughness

it joins the original airfoil tangentially. The lower nose domain modification was kept the same as on version M1, fig. 6. On this modification, the dolphin-shaped form was lost on the upper airfoil camber.

The obtained results were very satisfactory, compared to previous modifications M1 and M2. The calculated $C_{L,\max}$ for M3 was $C_{L,\max} = 1.33$, only 2% smaller than NACA's value 1.36, while $(C_L/C_D)_{\max} = 61.49$ was 8% larger than NACA's 56.75, tab. 1. Drag divergence on the M3's polar curve is practically the same as NACA's; the M3's drag coefficients are even a bit smaller at moderate C_L values.

Table 1. Variations from lift and drag coefficients and their ratios, with AoA α

NACA 2415 (standard roughness)				Original Dolphin 2415 (standard roughness)				Dolphin 2415 M4 (standard roughness)			
α [°]	C_L	C_D	C_L/C_D	α [°]	C_L	C_D	C_L/C_D	α [°]	C_L	C_D	C_L/C_D
–6	–0.41	0.01135	–36.12	–6	–0.38	0.04045	–9.39	–6	–0.50	0.01204	–41.53
–4	–0.21	0.01008	–20.83	–4	–0.24	0.02409	–9.96	–4	–0.27	0.01006	–26.84
–2	–0.02	**0.00953**	–2.10	–2	–0.02	0.01384	–1.45	–2	–0.03	**0.00928**	–3.23
0	0.18	0.00962	18.71	0	0.21	**0.00936**	22.44	0	0.21	0.00941	22.32
2	0.38	0.01038	36.61	2	0.44	0.01253	**35.12**	2	0.45	0.01039	43.31
4	0.59	0.01183	49.87	4	0.64	0.02118	30.22	4	0.69	0.01226	56.28
6	0.79	0.01408	56.11	6	0.76	0.03520	21.59	6	0.92	0.01522	**60.45**
8	0.98	0.01727	**56.75**	8	**0.81**	0.05452	14.86	8	1.13	0.02003	56.42
10	1.14	0.02176	52.39	10	0.80	0.08298	9.64	10	1.29	0.02817	45.79
12	1.28	0.02838	45.10	–	–	–	–	12	**1.36**	0.04099	33.18
14	**1.36**	0.03965	34.30	–	–	–	–	14	1.35	0.06198	21.78
16	1.32	0.06288	20.99	–	–	–	–	14.5	1.33	0.06913	19.24

The fourth modification: only drawback of the M3 modification was quite severe drag divergence at negative angles of attack. That means that this airfoil should not be appropriate for the Aerobatic airplane category, because it would require very high throttle settings in inverted flight. Since the application of elliptic contour on the front upper airfoil surface has solved the early drag divergence problems with versions M1 and M2, an obvious solution was to introduce yet another airfoil modification, the Dolphin 2415 M4. The upper elliptic arc was preserved from modification M3, while the lower surface modification form M1 has been replaced by lower elliptic arc, from the leading edge to the point $x = 0.29$ and $z = -0.0567667$, where it also joins the original Dolphin airfoil tangentially. By this final modification, the characteristic dolphin-like nose shape was lost, fig. 6. The M4 version, being elliptical in about 30% in the front, and original Dolphin in the remaining 70% of its contour, is a kind of a *semielliptical-dolphin* hybrid geometry.

The Dolphin 2415 M4 has $C_{L,\max} = 1.36$, which is equal to the NACA airfoil value. Its $C_{D,\min}$ is 2.6% smaller, while $(C_L/C_D)_{\max}$ is 6.5% higher than the corresponding values for NACA 2415, which are favorable trends. Also, the lift curve slope of M4 is even 22% larger than the NACA's, providing higher lifting efficiency per unit change of angle of attack (see also the corresponding values for the original Dolphin airfoil in tab. 2).

Table 2. Obtained changes $C_{L,\max}$, $C_{D,\min}$, $(C_L/C_D)_{\max}$ ratio, and lift curve slope (lift gradient), a, for the original Dolphin and its M4 modification

Airfoil	$C_{L,\max}$	Relative change	$C_{D,\min}$	Relative change	$(C_L/C_D)_{\max}$	Relative change	$a = dC_L/d\alpha$	Relative change
NACA 2415	1.36		0.00953		56.75		0.097	
Dolphin 2415 orig.	0.81	–40.4%	0.00936	–1.8%	35.12	–38.1%	0.102	+5.4%
Dolphin 2415 M4	1.36	0.0%	0.00928	–2.6%	60.45	+6.5%	0.118	+22.2%

As a summary, the Dolphin 2415 M4 has preserved the same calculated $C_{L,\max}$ as of the NACA 2415, while other aerodynamic parameters exceed to a moderate extent those of the NACA airfoil. The flow patterns around M4's nose are smooth both at negative and positive angles of attack (AoA), while the trailing edge separation is also quite similar to the NACA's pattern, fig. 8. Although the Dolphin-shaped nose could not have been preserved as a recognizable *trademark* of the geometry, the advantages of the original Dolphin's 70% rear domain combined with the two new semielliptical (upper and lower) nose segments, have made the M4

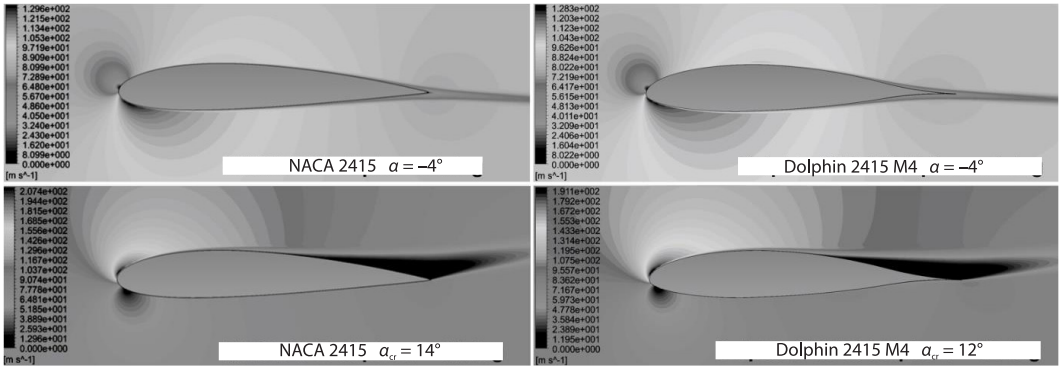

Figure 8. Velocity contours calculated for angles of attack $\alpha = -4°$, and the critical AoA $\alpha_{cr} = 14°$ for NACA 2415, and $\alpha_{cr} = 12°$ for the Dolphin 2415 M4 airfoil

a reasonable counterpart and *an acceptable* replacement for NACA 2415 in general aviation category. It also paves the way for many future investigations about the possibilities of applying the here explained design logic to improve the airfoils with other combinations of camber and thickness ratios, including the implementation of other nose modification contours, beside the elliptical.

Conclusion

The results presented in this paper have shown that the modified airfoil Dolphin 2415 M4 has improved aerodynamic characteristics in comparison to the original Dolphin 2415 airfoil and the classical NACA 2415. The original Dolphin airfoil was designed according to the mathematical model of Taposu [4, 5]. After the first numerical calculations of the original Dolphin 2415 and the obtained results, the aim was to improve the original Dolphin's characteristics in a wider range of angles of attack, by modifying its nose domain. The aerodynamic forces have performed the *natural optimization* of the airfoil geometry for a given AoA, which paved a way for further modifications. A modified version – M4 with a preserved 70% of the rear domain, has exceeded the original Dolphin 2415 and NACA 2415 aerodynamic characteristics. Numerical calculations have shown an increase in the lift-to-drag ratio, drag reduction, higher lift gradient, stall delay, smooth flow patterns around the leading edge for both- negative and positive AoA, and overall better performances, although the maximum lift has remained the same in version M4 and NACA 2415.

The Dolphin 2415 M4 has spawned a new airfoil geometry – a hybrid semi-elliptical Dolphin airfoil, suitable for general aviation applications with clearly presented improvements, which was the initial goal of this paper. In all of its development phases, the separated flow visualization in the sharp nose domain of the original Dolphin airfoil at different angles of attack has been successfully used as the primary source for the described airfoil geometry improvements, practically suggested by the nature. The natural flow visualization methodology presented and implemented in this paper, quite simple but also very efficient, can readily be generalized and applied to perform the geometry optimizations of many other categories of airfoils, and provide a wide range of further research possibilities.

Nomenclature

$g(x)$ – half-thickness distribution, [–]
L – lift force, [N]
D – drag force, [N]
C_L – lift coefficient, [–]
C_D – drag coefficient, [–]
L/D or C_L/C_D – lift-to-drag ratio, [–]
$(C_L/C_D)_{max}$ – maximum lift-to-drag ratio, [–]
$C_{L,max}$ – maximum lift coefficient, [–]
$C_{D,min}$ – minimum drag coefficient, [–]
$(r/c)_0$ – relative leading edge radius, [–]
$s(x)$ – skeleton line distribution function, [–]
$z_e(x)$ – suction surface, [–]
$z_i(x)$ – pressure surface, [–]
x_ζ – position of the maximum camber, [–]
x_ε – position of the maximum thickness, [–]

Greek symbols

α – AoA, incidence angle, [°]
α_{cr} – critical angle of attack, [°]
ε – half- thickness of the airfoil, [–]
ζ – camber, [–]

Acronyms

AoA – angle of attack
M1 – first modification
M2 – second modification
M3 – third modification
M4 – fourth modification

References

[1] Vincent, J. F., *et al.*, Biomimetics: Its Practice and Theory, *Journal of the Royal Society, Interface*, *3,* (2006), 9, pp. 471-482

[2] Gibbs- Smith., C., *Sir George Cayley's Aeronautics 1796-1855*, Science Museum Her Majesty's Stationery Office, London, UK, 1962
[3] Huang, W., *et al.*, Research on Aerodynamic Performance of a Novel Dolphin Head-Shaped Bionic Airfoil, *Energy*, *214* (2021), 118179
[4] Taposu, I., Spataru, P., About the Experimental Results of a Dolphin Profile at Low Speeds, *Proceedings*, 18th Applied Aerodynamics Conference, Denver, Col., USA, 2000, pp. 762-771
[5] Taposu, I., *The Dolphin Profiles. A new Concept in Aerodynamics,* (in Romanian), S.C. Editura Technica S.A., Bucharest, Romania, 2002
[6] Berbente, C., Danaila, S., On the Aerodynamic Characteristics of a Class of Airfoils with Continuous Curvature at Subsonic, Transonic and Supersonic Regimes, *Scientific Bulletin U. P. B., 69* (2007), 1, pp. 15-28
[7] Ivanov, T., *et al*, Influence of Selected Turbulence Model on the Optimization of a Class-Shape Transformation Parameterized Airfoil, *Thermal Science*, *21* (2017), pp. 737-744
[8] Peigin, S., *et al.*, Unmanned Air Vehicle 3-D Wing Aerodynamical Design and Algorithm Stability with Respect to Initial Shape, *Thermal Science*, *23* (2019), Suppl. 2, pp. S599-S605
[9] Ocokoljic, G., *et al.*, Aerodynamic Shape Optimization of Guided Missile Based on Wind Tunnel Testing and Computational Fluid Dynamics Simulation, *Thermal Science*, *21* (2017), 3, pp. 1543-1554
[10] Abbott, I. H., *et al.*, Summary of Airfoil Data Report NACA Report No. 824, National Advisory Committee for Aeronautics, USA, 1945
[11] ***, ANSYS FLUENT 16.0, Theory Guide, ANSYS Inc, Canonsburg, PA, 2015
[12] Menter, F. R., Two-Equation Eddy-Viscosity Turbulence Models for Engineering Applications, *AIAA Journal*, *32* (1994), 8, pp. 1598-1605
[13] ***, Turbulence Modelling Resource, NASA Langley Research Center, https://turbmodels.larc.nasa.gov/sst.html
[14] Menter, F. R., Improved Two-Equation k-ω Turbulence Models for Aerodynamic Flows, NASA STI/Recon Technical Report, 1992
[15] Kostić, O., Computational Simulation of Air-flow in Supersonic Nozzle with Obstacle at Exit, (in Serbian), Ph. D. thesis, University of Belgrade, Faculty of Mechanical Engineering, Belgrade, Serbia, 2016
[16] Kostić, O., *et al*, The CFD Modelling of Supersonic Air-Flow Generated by 2-D Nozzle with and without an Obstacle at the Exit Section, *FME Transactions*, *42* (2015), 2, pp. 107-113
[17] Kostić, O., *et al*, Comparative CFD Analyses of a 2-D Supersonic Nozzle Flow with Jet Tab and Jet Vane, *Tehnički vjesnik – Technical Gazette, 24* (2017), 5., pp. 1335-1344

Paper submitted: May 15, 2021
Paper revised: May 28, 2021
Paper accepted: June 1, 2021